processes

MDPI

Article

AuNRs-MIL-100(Fe) as Surface-Enhanced Raman Spectroscopy Substrates for Rapid and Sensitive Analysis of Malachite Green in Fishpond Water

Yiming Ou [1], Jianlan Chen [1], Yishan Song [2] and Keqiang Lai [2,*]

[1] School of Food and Pharmacy, Shanghai Zhongqiao Vocational and Technical University, Shanghai 201514, China; ouyiming1201@126.com (Y.O.)
[2] College of Food Science and Technology, Shanghai Ocean University, Shanghai 201306, China
* Correspondence: kqlai@shou.edu.cn; Tel.: +86-21-6190-0372

Abstract

Malachite green (MG) is a prohibited aquaculture biocide. As its residues in fish can be confirmed only after accumulation in the tissue, early identification of illegal use depends on measuring the rearing water. Here, gold nanorods (AuNRs) were integrated with MIL-100(Fe) to give an anisotropic substrate for the surface-enhanced Raman scattering (SERS) determination of MG in fishpond water. AuNRs of three aspect ratios (2.4, 2.85 and 3.99) were prepared by a seed-mediated route, and the AR 3.99 exhibited the optimal SERS enhancement, giving a signal 56% stronger than the spherical AuNPs-MIL-100(Fe) counterpart at the same Au concentration. The response was linear from 0.1 to 10 μg/L and, in spiked fishpond water, gave $R^2 = 0.966$ and recoveries of 89.6–100.9% (RSD 3.7–9.1%), with no extraction or pre-concentration step. The method is therefore suited to rapid routine monitoring of aquaculture water and to food safety supervision.

Keywords: surface-enhanced Raman spectroscopy; gold nanorods; metal–organic framework; malachite green; fishpond water

1. Introduction

Malachite green (MG) is a cationic triphenylmethane dye that has been used for decades in aquaculture as a biocide, owing to its efficient action against fungal attacks, protozoan infections and other diseases of aquatic organisms, and it has additionally served as a food colouring agent, a medical disinfectant and an industrial dye for silk, wool and paper [1]. These benefits were, however, accompanied by a severe toxicological profile: MG is reduced in fish to its metabolite leucomalachite green (LMG), and both compounds persist for extended periods in aquatic animal tissues and in the rearing environment, with reported effects including carcinogenesis, mutagenesis, chromosomal breakage, teratogenicity and respiratory toxicity [2]. MG has consequently been banned in China for all food animals in 2002, where it remains on the current national list of prohibited drugs. Notwithstanding these prohibitions, MG is still detected in aquaculture products and in the water in which they are reared [3].

Contamination of the water body precedes any accumulation of residues in the fish themselves, because MG is applied directly to the rearing water. Water is therefore the matrix in which illegal use can be detected earliest, whereas the official methods are defined for the fish themselves: the Chinese national standard GB/T 19857-2005 determines MG in the edible tissues of aquatic products, with detection limits of 0.5 μg/kg by LC–MS/MS

Check for updates

Academic Editors: Konstantinos I. Chatzipanagis and Dimitrios Palles

Received: 24 August 2026
Revised: 21 October 2026
Accepted: 29 October 2026
Published: 3 November 2026

Copyright: © 2026 by the authors. Licensee MDPI, Basel, Switzerland. This article is an open access article distributed under the terms and conditions of the Creative Commons Attribution (CC BY) license.

and 2.0 μg/kg by HPLC, so that residues are confirmed only after they have accumulated in the fish [4]. MG released into the water persists there and is transferred to aquatic organisms through the food chain, ultimately disturbing the balance and stability of aquatic ecosystems [5]; direct determination of MG in water has consequently attracted continued attention [6,7]. Rapid and accurate determination of trace MG in these waters would allow illegal use to be identified early rather than established after the fact.

Surface-enhanced Raman scattering (SERS) is well suited to meeting this requirement. It is a highly sensitive analytical technique that enhances the Raman signals of target molecules adsorbed on rough metal surfaces, enabling the trace detection of substances in complex environments. It additionally offers short measurement times and fingerprint specificity, and in many cases requires little or no sample pretreatment. The enhancement is governed by localized surface plasmon resonance (LSPR) and depends on the shape, structure, size and other characteristics of the metal nanostructures [8]. Both the material and the geometry of the plasmonic nanostructure have therefore been varied extensively in the search for sensitive substrates for MG.

The reported performance of such substrates spans several orders of magnitude (Table 1). Citrate-reduced gold nanospheres of different sizes were synthesized, and particles of 36 ± 4 nm gave the strongest enhancement, with MG in aquaculture water detected down to 10^{-7} M [9]. Magnetic collection has likewise proved an effective way of raising the local analyte and hot-spot density: Au-coated Fe_3O_4 composite nanospheres (Fe_3O_4@Au MCS) prepared by seed-mediated growth with iterative reduction reached a comparable 10^{-7} M in aquaculture water while remaining recoverable with an external magnet [10]. Silver-coated urchin-like gold nanoparticles reach about 0.9 μg/L in aquaculture water [11]; and a molecularly imprinted sensor built on gold nanostars reaches 3.5 μg/L in seawater [12]. Rod-shaped gold has been examined as well: on standing AuNRs, MG and crystal violet were determined in fish down to 1 μg/kg, although the two congeners could only be separated after multivariate treatment of the spectra [13]. These results confirm the potential of SERS for MG; nevertheless, two obstacles remain. First, the enhancement decays sharply beyond about 10 nm from the metal surface, so the analyte must be brought close to, and retained at, the metal [14], while gold and silver nanoparticles are prone to aggregation during both preparation and detection, which compromises signal quality and stability [15,16]. Second, most organic analytes (including MG) exhibit low affinity for metal surfaces, and complex sample matrices further impede the efficient adsorption of MG molecules, posing significant challenges for the sensitive detection of trace MG using metal-based SERS substrates [17].

Metal–organic frameworks (MOFs) offer a direct remedy: their large specific surface area, ultra-high porosity and tailorable structure and functionality [18–20] enable the selective adsorption and preconcentration of the target, so that integrating a MOF with a noble metal enhances the Raman signal synergistically, as demonstrated for several MOF–metal composites [21] and in recent MOF-based sensors for aqueous pollutants [22]. MOF–metal composites have furthermore been exploited for other purposes, including the catalytic degradation of MG in polluted water [23] and alternative sensing modalities [24].

On the other hand, the plasmonic component efficiency can be raised by moving from spherical to anisotropic nanostructures: spherical nanoparticles display a single LSPR whereas anisotropic ones display two or more distinct modes [25], and gold nanorods (AuNRs) are especially attractive in this respect because their longitudinal LSPR can be tuned from the visible to the near-infrared [26]; they are obtained in high yield by well-established seed-mediated routes [27], and their optical properties and stability have been extensively documented [28,29]. Anisotropic rod-shaped silver nanostructures have likewise been explored as SERS substrates [30,31]. In our previous work we combined MIL-

100(Fe) with spherical gold nanoparticles: the resulting AuNPs@MIL-100(Fe) composite synergistically enhanced the Raman signal and enabled the determination of MG in fish at 0.1 μg/kg [32].

Table 1. Comparison of representative SERS substrates for the determination of malachite green (MG).

Substrate	Preparation Method	Au Morphology	Matrix	LOD	Ref.
gold nanospheres	sodium citrate reduction	sphere	aquaculture water	10^{-7} M	[9]
Fe_3O_4@Au MCS	seed-mediated growth and iterative reduction	sphere	aquaculture water	10^{-7} M	[10]
Ag-coated urchin-like AuNPs	one-pot synthesis; Ag coating	hollow, branched	aquaculture water	0.9 μg/L	[11]
Au nanostars + imprinted polydopamine	one-pot synthesis; polydopamine imprinting	star	seawater	3.5 μg/L	[12]
Standing AuNRs	AuNRs assembled standing on a substrate	rod	fish (extract)	1 μg/kg	[13]
Fe_3O_4@ZIF-67@Ag	self-assembly of AgNPs on ZIF-67 shell	nanosphere	fishpond water	8.7×10^{-10} M	[21]
AuNPs@MIL-100(Fe)	electrostatic adsorption	sphere	Nine fish tissue	0.003–0.088 μg/kg	[32]

Herein, a size-tunable AuNRs-MIL-100(Fe) composite was fabricated as a high-performance SERS substrate, aiming to achieve sensitive and rapid detection of MG residues in fishpond water. MIL-100(Fe) was selected as the MOF component due to its large specific surface area and excellent adsorption capacity, which facilitates the concentration of MG molecules at the "hot spots" formed by AuNRs. The proposed composite substrate combined the dual advantages of AuNRs and MIL-100(Fe), thereby improving the sensitivity and selectivity of SERS detection. Notably, the developed method eliminates the need for complex sample pretreatment, enabling convenient and on-site applicable detection of MG residues. The study not only provides a strategy for designing MOF-based SERS substrates integrated with anisotropic gold nanoparticles, but also demonstrates that such substrates permit the direct screening of aquaculture water, providing an early warning of MG contamination.

2. Materials and Methods

2.1. Chemicals and Materials

Reagents were the same as those used in our earlier work [32] and are grouped below by role. MOF synthesis: $Fe(NO_3)_3 \cdot 9H_2O$ (AR, 98.5%; Aladdin Reagent Co., Shanghai, China) and 1,3,5-benzenetricarboxylic acid (H_3BTC, AR, 98%; J&K Scientific Ltd., Logan, UT, USA). AuNR synthesis: $HAuCl_4$ (99.9%; Sigma-Aldrich, St. Louis, MO, USA), cetyltrimethylammonium bromide (CTAB, 98%) and trisodium citrate dihydrate ($Na_3C_6H_5O_7 \cdot 2H_2O$, AR, 99%) (both J&K Scientific), together with $NaBH_4$, $AgNO_3$, HCl and L-ascorbic acid (AR; Sinopharm Chemical Reagent Co. Ltd., Shanghai, China). Analyte: malachite green (MG, 99%; Sigma-Aldrich). Other chemicals were all of analytical grade and obtained from Sinopharm Chemical Reagent Co. Ltd., Shanghai, China.

2.2. Preparation of AuNRs with Different ARs

AuNRs with different ARs were synthesized via a two-step seed-mediated method [33], consisting of seed preparation and AuNR growth, as detailed below: First, 2.5 mL of $HAuCl_4$ solution (0.5 mM) and 2.5 mL of CTAB solution (0.2 M, preheated to 60 °C) were

mixed uniformly in a beaker under magnetic stirring (1100 rpm) for 10 min to facilitate isotropic growth of gold nuclei. Subsequently, 300 μL of freshly prepared $NaBH_4$ solution (0.01 M, ice-bath cooled) was rapidly injected into the mixture under continuous stirring. The resulting solution was transferred to a constant temperature and humidity chamber (29 °C, 70% relative humidity) and allowed to age for 1.5 h, yielding a brownish-yellow gold seed solution that was stored for subsequent use. Second, for the growth solution preparation: 10 mL of CTAB solution (0.2 M, preheated to 60 °C) and 10 mL of $HAuCl_4$ solution (1 mM) were mixed under magnetic stirring (1100 rpm) for 10 min, during which CTAB spontaneously self-assembled into rod-like micelles in the aqueous phase. Different volumes of $AgNO_3$ solution (0.01 M, 50, 140, or 240 μL) were sequentially added to the mixture, followed by continuous stirring at 1100 rpm for 5 min. Next, 0.2 mL of HCl solution (2 M) was introduced, and the mixture was stirred for an additional 5 min (1100 rpm). Afterward, 0.16 mL of L-ascorbic acid solution (0.1 M) was added as a mild reducing agent, resulting in a color change from orange-yellow to colorless—indicating the formation of the AuNR growth solution. Finally, 70 μL of the as-prepared gold seed solution was injected into the growth solution. The mixture was incubated in a constant temperature and humidity chamber (29 °C, 70% relative humidity) for 16 h, leading to the formation of AuNRs and a corresponding color change to dark brown. The synthesized AuNRs were purified via three rounds of centrifugation (8000 rpm, 10 min) to remove excess CTAB. The resulting pellets were redispersed in different volumes of ultrapure water (0.5–10 mL) and stored at 4 °C for subsequent experiments.

2.3. Preparation and Characterization of AuNRs-MIL-100(Fe)

A MIL-100(Fe) suspension (1 mg/mL, methanol-water mixed solution) was prepared according to a previously reported protocol [32], followed by ultrasonication for 40 min to ensure uniform dispersion. For the preparation and optimization of the SERS composite substrate, the as-prepared MIL-100(Fe) suspension and AuNRs were incubated at 4 °C for 60 min at different volume ratios. Ultraviolet-visible (UV-Vis) absorption spectra of the AuNR samples were recorded using a spectrophotometer (UV300PC, Mepro Delta Instruments, Shanghai, China) in the wavelength range of 400–900 nm. Transmission electron microscopy (TEM, JEM-2100F, JEOL, Akishima, Tokyo, Japan) was employed to characterize the surface morphology of the samples and calculate the average aspect ratio of AuNRs. Energy-dispersive X-ray spectroscopy (EDX, Aztec X-MaxN 80, Oxford Instruments, Abingdon, UK) was utilized to analyze the elemental composition of the SERS composite substrate.

2.4. Sample Preparation and SERS Measurement

To evaluate the SERS performance of the AuNRs-MIL-100(Fe) composite substrate, a series of malachite green (MG) standard solutions with gradient concentrations (0.1–10 μg/L, ppb) were prepared using ultrapure water. Fishpond water samples were collected from a local fishpond in Shanghai (random sampling site) and stored at 4 °C prior to use. For spiked sample preparation, the fishpond water samples were spiked with MG to obtain gradient concentrations, followed by filtration through a 0.45 μm polyvinylidene fluoride (PVDF) filter (SCAA-103, 13 mm) to remove particulate impurities before SERS measurements.

SERS spectra were acquired using a Raman spectrometer (Nicolet DXR, Thermo Fisher Scientific, Waltham, MA, USA) equipped with a 633 nm He–Ne laser (10× objective lens, 2 mW laser power). For sample preparation, the as-prepared AuNRs-MIL-100(Fe) composite solution was mixed with MG solutions (standard or spiked samples) at a volume ratio of 1:3 (v/v). After vortex mixing for 30 s to ensure sufficient interaction, 5 μL of the mixture was deposited onto clean glass slides and dried at 45 °C for 20 min. SERS spectra

were recorded from 10 randomly selected positions on each sample. Each spectrum was obtained by averaging three scans, and the exposure time for each scan was 5 s.

To assess the reproducibility of the composite substrate, three independent batches of AuNRs-MIL-100(Fe) were fabricated under identical experimental conditions. Each batch was mixed with a 20 μg/L MG standard solution for SERS testing. The relative standard deviation (RSD) of the characteristic peak intensities was calculated both within a single batch (intra-batch) and across the three batches (inter-batch).

2.5. Data Analysis

OMNIC for Dispersive Raman 9.7 (Thermo Nicolet Corp., Madison, WI, USA) was utilized for raw spectral data processing, while Origin 2024 software was employed for subsequent SERS spectral analysis—including baseline correction, linear regression fitting, and relative standard deviation (RSD) calculation.

Data analysis was carried out following the protocol established in our previous work [32]. Calibration curves were constructed by plotting the mean SERS intensity of the 1617 cm^{-1} band, recorded from ten positions on each specimen, against the MG concentration over the range examined, and fitted by linear regression; the same procedure was applied to the standard solutions and to the spiked fishpond water samples.

3. Results and Discussion

3.1. Synthesis and Characterization of AuNRs-MIL-100(Fe)

This section traces AuNR growth from mechanism to morphology, and then to their integration with MIL-100(Fe). Early theories proposed that rod-shaped CTAB micelles in the reaction system might serve as soft templates for the formation of AuNRs, as illustrated in Figure 1a, where the AuNRs were either single-crystalline or penta-crystalline. However, during synthesis, the seed particles (4–6 nm in diameter) were significantly larger than CTAB micelles, making it implausible for micelles to act as soft templates capable of encapsulating the seed particles and promoting their growth [34]. Furthermore, AuNRs could still form when the CTAB concentration was below the critical micelle concentration, provided that the bromide ion concentration was maintained at 0.1 M. As a result, the "zipper mechanism" was proposed to explain the anisotropic growth of AuNRs [35]. In this model, CTAB was strongly adsorbed onto the lateral surfaces of growing gold nanoparticles, as illustrated in Figure 1b, forming a bilayer that restricts the access of Au(I) to these surfaces. Consequently, regardless of whether the nanoparticles were single-crystalline or penta-crystalline, growth was favored on the tip facets of AuNRs. This is because the CTAB adlayer on the tip surfaces is sparser, allowing easier access for gold deposition [36]. The AR is therefore governed mainly by additives that perturb this surfactant layer, above all the Ag^+/Br^- balance—which is why the $AgNO_3$ dosage was varied here.

Because AR is set by this growth mechanism, it should leave a clear signature in the plasmonic response; UV–Vis spectra of the three samples were therefore recorded. As shown in Figure 2, the three AuNR samples exhibited two plasmon resonance bands: a transverse plasmon band at approximately 520 nm and longitudinal plasmon bands at 621 nm, 785 nm, and 721 nm, corresponding to the addition of 50 μL, 140 μL, and 240 μL of silver nitrate ($AgNO_3$), respectively. The longitudinal band first underwent a red shift followed by a blue shift. As previously reported, during AuNR synthesis, Ag^+ combines with Br^- derived from CTAB to form AgBr, which was deposited on the lateral surfaces of AuNRs. This process inhibited the transverse growth of AuNRs and reduced their overall growth rate, thereby facilitating the preferential deposition of gold atoms at energetically favorable sites and the optimization of AuNR structure and morphology [37]. However, excessive $AgNO_3$ addition was found to suppress AuNR growth [38–40].

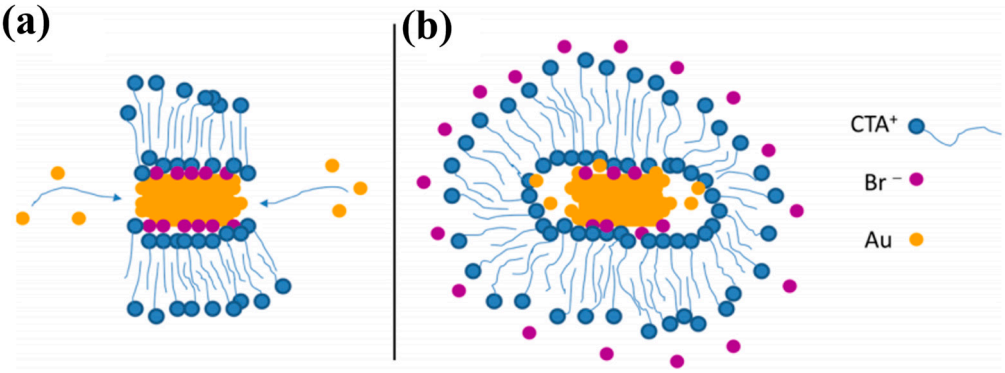


Figure 1. (**a**) Illustration of AuNR's zipper growth mechanism; (**b**) the role of soft templates in the growth process.

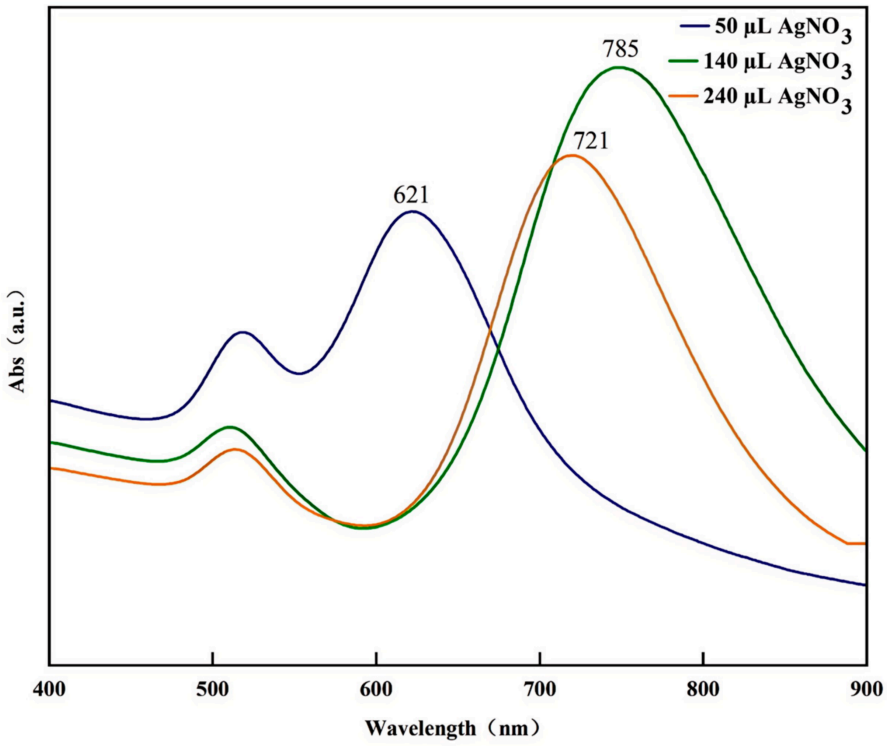


Figure 2. UV–Vis of AuNRs synthesized by adding 50, 140 and 240 μL $AgNO_3$.

Figure 3 further corroborated this observation. As the volume of $AgNO_3$ added increased from 50 μL to 140 μL, the AR of AuNRs increased from 2.4 (length: 54.17 ± 1.1 nm; diameter: 22.92 ± 2.9 nm) to 3.99 (length: 66.67 ± 2.08 nm; diameter: 16.67 ± 2.08 nm). As the volume was further increased to 240 μL, the AR decreased to 2.85 (length: 77.08 ± 2.0 nm; diameter: 27.08 ± 2.08 nm), accompanied by a reduced AuNR yield and the formation of spherical particles. Overall, the addition of 140 μL $AgNO_3$ yielded AuNRs with the highest longitudinal plasmon peak intensity, high yield, and excellent dispersibility. Subsequently, energy-dispersive X-ray spectroscopy (EDX) elemental mapping analysis (Figure 4) further confirmed the successful integration of AuNRs with MOF materials. Elements of Au, Fe, O, and C were uniformly distributed throughout the nanostructure, providing a solid experimental foundation for the subsequent adsorption of malachite green (MG). The two components are thus integrated within a single composite; how they are held together is addressed next.

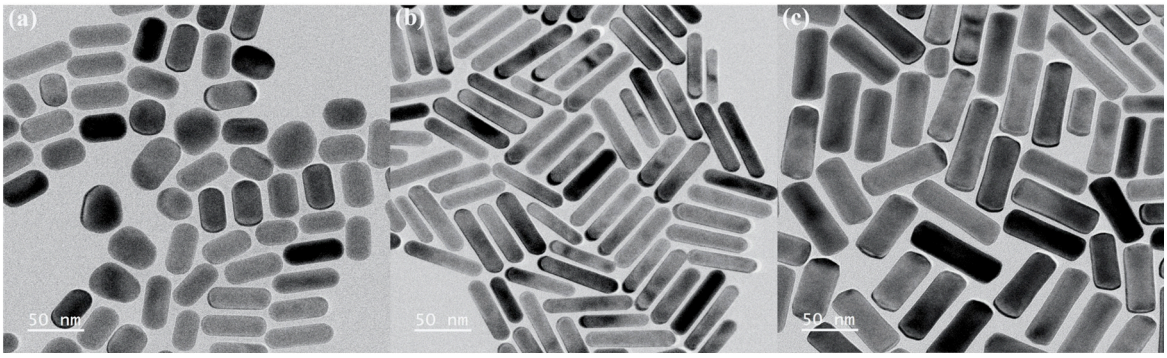


Figure 3. TEM images of AuNRs with different ARs obtained by adding different volumes of $AgNO_3$: (**a**) 50 µL, (**b**) 140 µL, and (**c**) 240 µL.

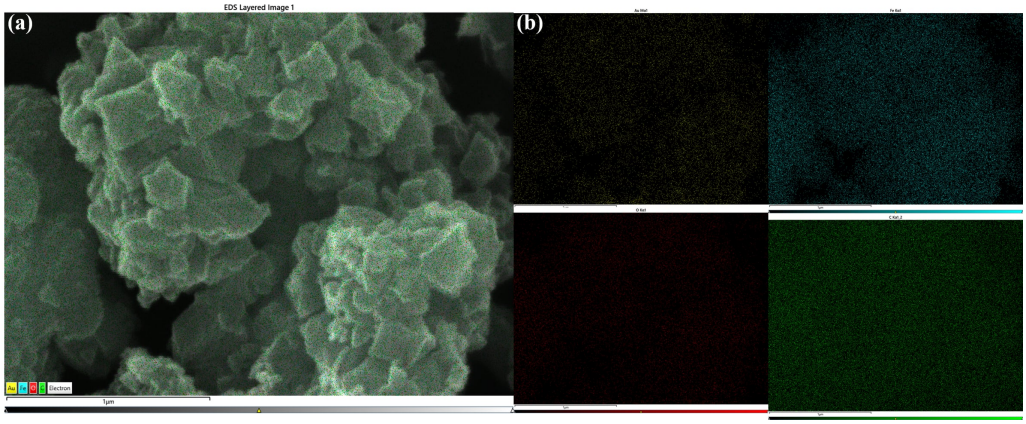


Figure 4. SEM image (**a**) and corresponding EDX elemental mapping (**b**) of the AuNRs-MIL-100(Fe) composite.

The combination of AuNRs with MIL-100(Fe) is driven primarily by electrostatic self-assembly. Surfactant-mediated electrostatic assembly is a well-established route to Au–MOF hybrids, which combine plasmonic enhancement with adsorptive preconcentration [18,41]. AuNRs prepared by the seed-mediated route retain a bilayer of cetyltrimethylammonium bromide (CTAB) on their surface, whose quaternary ammonium headgroups impart a strongly positive surface charge [42]. MIL-100(Fe) is an iron(III) trimesate framework, and the exposed carboxylate groups together with the aquo and hydroxo iron sites render its surface negatively charged in aqueous suspension. Mixing the two suspensions therefore leads to spontaneous electrostatic assembly, in which the cationic AuNRs deposit onto the anionic MOF crystallites. This primary interaction is reinforced by van der Waals attraction between the CTAB adlayer and the framework surface, and by coordination-type interactions in which coordinatively unsaturated Fe(III) sites act as Lewis acid centres towards the adsorbed surfactant [43]. The resulting architecture is synergistic: the MOF concentrates MG from solution through its porosity and holds it in the vicinity of the metal surface.

The assembly described above was carried out at 4 °C, a condition that proves advantageous for three reasons. Low-temperature assembly is likewise a recognised way to preserve both colloidal stability and framework integrity [43]. First, Brownian transport is markedly slowed at low temperature, so that particle collisions occur gently and the composite assembles progressively rather than undergoing rapid, uncontrolled flocculation; this yields a more uniform decoration of the MOF surface, which is directly relevant to the uniformity of the SERS hotspots. Second, CTAB adsorbed on the AuNR surface is less prone to desorption below its Krafft temperature, so the rod-stabilising bilayer remains

intact throughout deposition and the nanorods retain their morphology instead of fusing or reshaping. Third, MIL-100(Fe) is less susceptible to hydrolytic degradation and structural reorganisation at low temperature, so its porosity and adsorption sites are preserved. Working at 4 °C thus protects both components of the composite and gives a reproducible, uniformly decorated substrate on which the subsequent SERS performance depends.

3.2. Optimization of the AuNRs-MIL-100(Fe) Substrate

To optimize the SERS performance of the AuNRs-MIL-100(Fe) composite substrate, three key parameters were evaluated: the AR of AuNRs, the dilution volume of the AuNRs suspension, and the volume ratio of AuNRs to MIL-100(Fe). The AR is considered first because it sets the position of the longitudinal plasmon band and therefore determines how well the excitation and the Stokes-shifted frequencies are matched to it. Consistent with this expectation, the substrate integrated with AuNRs of AR 3.99 exhibited the strongest SERS enhancement, outperforming those with ARs of 2.4 and 2.85 (Figure 5a). The criterion applied here is not a simple matching of the plasmon band to the 633 nm laser line. The SERS intensity scales as the product of the local-field enhancement at the excitation frequency and at the Stokes-scattered frequency, $G \propto |E_loc(\omega_L)|^2 |E_loc(\omega_S)|^2$ [44], and a longitudinal plasmon band that overlaps the excitation source has been shown to raise the enhancement by 10–10^2 times [45]. The relevant condition is therefore that both frequencies fall within the longitudinal plasmon band of the nanorods, rather than that the laser alone lies close to the band maximum. For the band used for quantification (1617 cm^{-1}), the Stokes line excited at 633 nm appears near 705 nm. The rods prepared with 50 µL $AgNO_3$ (AR 2.4) have their longitudinal resonance at 621 nm (Figure 3). The laser is therefore nearly on resonance, but the 705 nm Stokes radiation lies about 84 nm to the red of the band maximum, outside the region where the local field is appreciably enhanced, so the second factor in the product remains small. Those prepared with 140 µL (AR 3.99) place the resonance at 785 nm (Figure 3), so that both the 633 nm excitation and the ≈705 nm Stokes emission fall within the longitudinal band, giving a substantially larger product. This account is reinforced by two further observations: anisotropic particles exhibit a pronounced lightning-rod effect, so rods with higher AR sustain stronger local-field confinement at their tips, and the same rods also gave the highest longitudinal plasmon intensity, the best yield and the least spherical by-product (Figures 2 and 3) [46,47]. The AR 3.99 rods were therefore adopted for all subsequent optimisation.

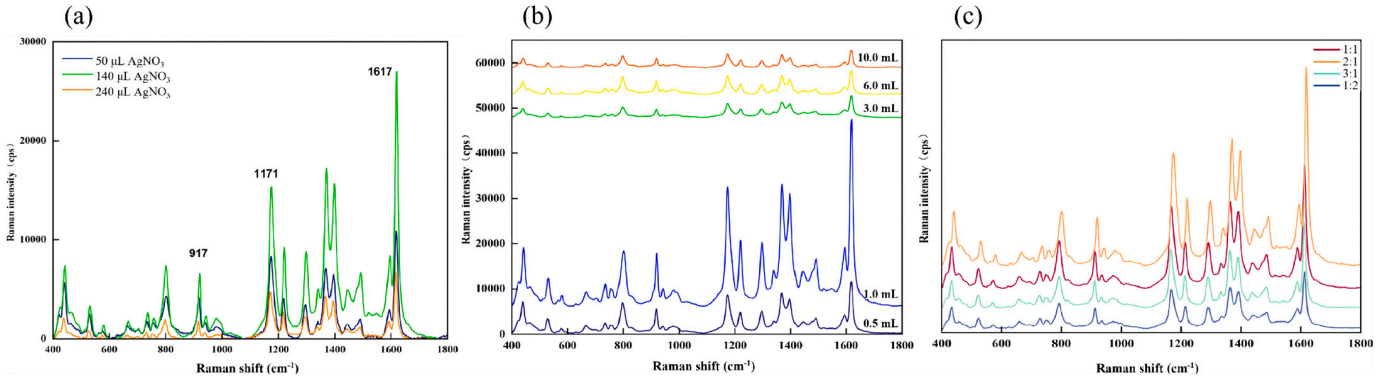


Figure 5. Ramanspectra of 20 µg/L MG standard solution on AuNRs-MIL-100(Fe) substrates with (**a**) different AuNRs, (**b**) different dilution volumes, and (**c**) different substrate ratios.

Figure 5b shows the influence of different dilution volumes (0.5, 1, 3, 6, and 10 mL) of the AuNRs suspension on SERS performance. The SERS signal intensity reached its maximum at a dilution volume of 1 mL. A too-small dilution volume results in a high

AuNR concentration, causing aggregation and stacking of AuNRs and thereby reducing the number of effective SERS "hot spots." In contrast, an excessively large dilution volume separates AuNRs too far apart, also decreasing the hot spot density. Using the optimal 1 mL diluted AuNRs suspension, SERS detection was conducted at different AuNRs-to-MIL-100(Fe) volume ratios (1:1, 2:1, 3:1, 1:2). The strongest Raman signal was achieved at a 2:1 ratio (Figure 5c), which is consistent with the findings for AuNPs combined with MIL-100(Fe) [32]. An excessively high proportion of AuNRs can occupy the active binding sites on MIL-100(Fe), induce AuNR aggregation, and hinder the effective adsorption of probe molecules (MG). Conversely, an overabundance of MIL-100(Fe) leads to insufficient generation of "hot spots"—a critical factor for Raman signal enhancement.

3.3. Analytical Performance of the AuNRs-MIL-100(Fe) Substrate

Under the optimized substrate conditions, the analytical performance of the SERS sensing system was evaluated in terms of reproducibility and linearity. The characteristic peaks of MG at 917 cm^{-1},1171 cm^{-1} and 1617 cm^{-1} were selected to assess the linearity of SERS sensing. Figure 6 showed that the SERS intensity at the characteristic peak at 1617 cm^{-1} of the AuNRs-MIL-100(Fe) substrate was 56% stronger than that of the previously reported AuNPs-MIL-100(Fe) substrate [32], confirming the superior detection performance of the AuNR-based substrate. Table 2 summarises these characteristic bands together with their vibrational assignments [48].

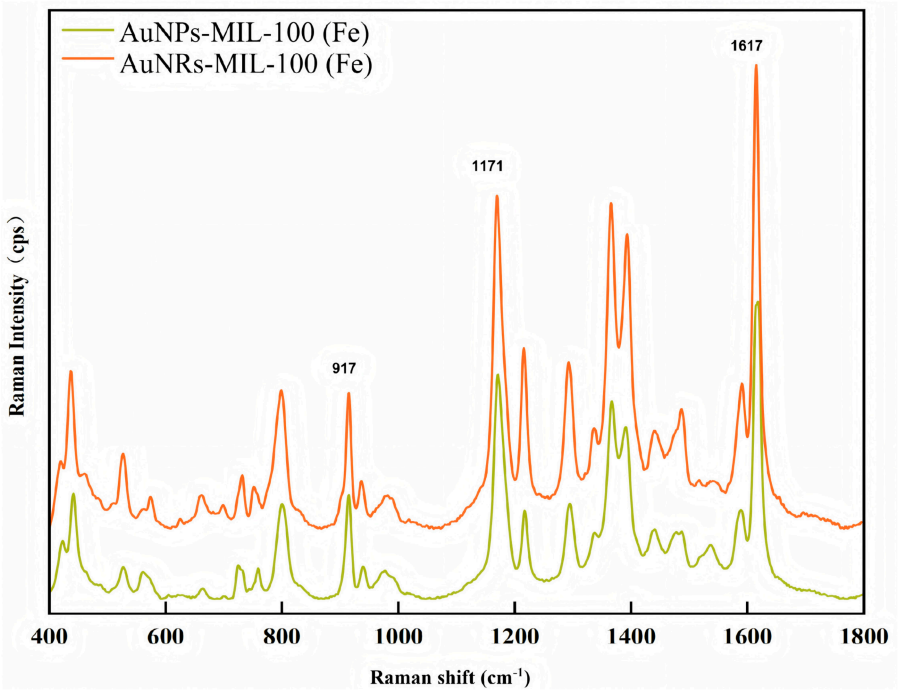


Figure 6. Raman spectra of 10 μg/L MG detected by AuNPs-MIL-100(Fe) and AuNRs-MIL-100(Fe) substrates with the same Au concentration.

Theoretically, the intense electric fields concentrated at the tips of AuNRs significantly enhanced SERS signals, endowing the system with high sensitivity for low-concentration analytes. Reproducibility was assessed by calculating the relative standard deviation (RSD) of the SERS signal at 1617 cm^{-1}. For each batch, the SERS spectra were recorded from 10 randomly selected positions on a dried specimen, and three independent batches were prepared under identical conditions; thus, the intra-batch RSD (n = 10 positions per batch) and the inter-batch RSD (n = 3 batches) were evaluated. The intra-batch RSD was 19.2%, while the inter-batch RSD—derived from three independently prepared sub-

strate batches—was 12.9%, and the comparable intra- and inter-batch variations confirm the acceptable reproducibility of the AuNRs-MIL-100(Fe) substrate (Figure 7). The slightly higher intra-batch RSD is mainly attributed to position-to-position variation across different SERS "hotspots" on the same specimen, whereas the inter-batch RSD reflects batch-to-batch variation in the averaged substrate signals.

Table 2. Assignments of the characteristic Raman bands of malachite green (MG) (Adapted from [48]).

Raman Shift (cm^{-1})	Band Assignment
440	γ (phenyl–C–phenyl)
800	γ (C–H)
917	Ring-breathing
1171	δ (C–H)
1368	*ν*ip (N–phenyl), *ν*ip (C–C)
1617	*ν*ip (C–C)

Abbreviations: ν = stretching; δ = in-plane bending; γ = out-of-plane bending; ip = in-plane.

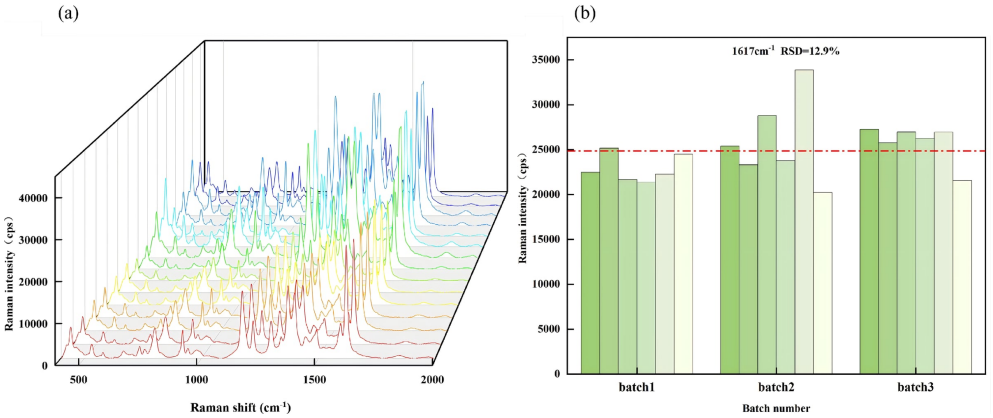


Figure 7. Sensingperformance of SERS substrate on MG reproducibility.

The linear range of the method was determined by detecting MG standard solutions with concentrations of 0.1, 0.5, 1, 5 and 10 μg/L. As shown in Figure 8, a good linear relationship was observed between the SERS intensity at 1617 cm^{-1} and MG concentration in the range of 0.1–10 μg/L, with a coefficient of determination (R^2) of 0.986. These results demonstrate the reliability of the AuNRs-MIL-100(Fe) substrate for the quantitative determination of MG over this range.

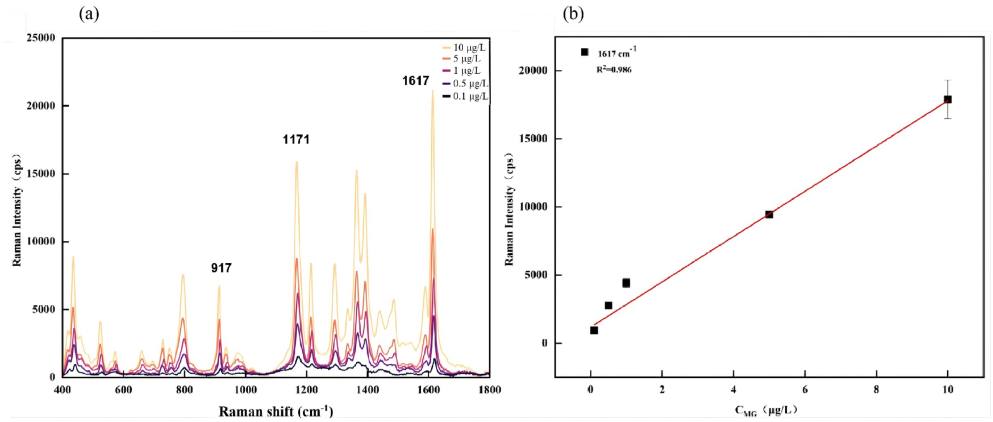


Figure 8. (**a**) SERS spectra of different MG standard solutions using AuNRs-MIL-100(Fe) substrates; (**b**) linear correlation curve between MG concentration and the intensity of its characteristic peak.

3.4. Detection of MG in Fishpond Water

The matrix background was assessed prior to quantification by acquiring SERS spectra of blank (unspiked) fishpond water. No bands assignable to MG were detected at 917, 1171 or 1617 cm^{-1}, confirming that MG was not detectable in the collected samples and that no spectral interference arises from the water matrix. SERS spectra of fishpond water spiked at different MG concentrations are shown in Figure 9a. The intensity at 1617 cm^{-1} scales linearly with the spiked MG concentration over the range investigated (Figure 9b), yielding a coefficient of determination (R^2) of 0.966. Such linearity over the measured concentration range indicates that adsorption of MG onto the AuNRs-MIL-100(Fe) substrate remains in a regime where the SERS response is proportional to analyte coverage, which underpins the quantitative use of the 1617 cm^{-1} band.

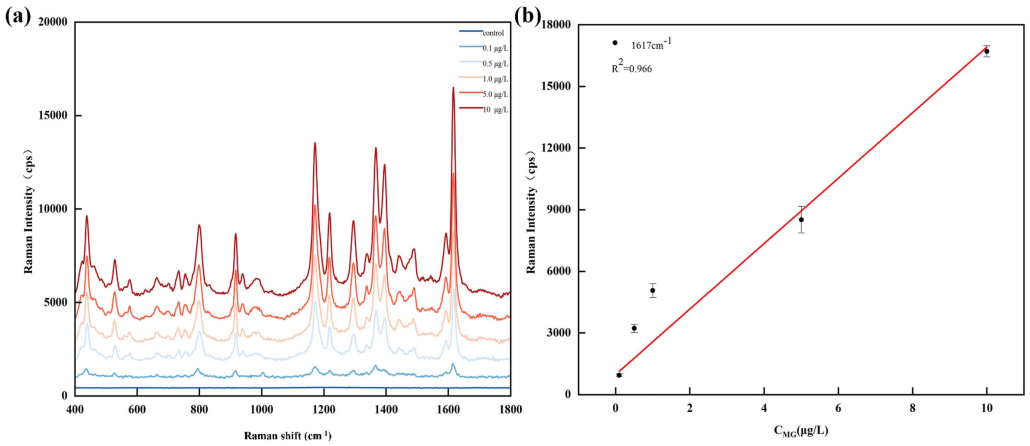


Figure 9. (**a**) SERS spectra of different concentrations of MG in fishpond water; (**b**) linear correlation between MG and characteristic peak intensity (1617 cm^{-1}).

The concentration range examined here is placed in context by the levels reported for the field. In a survey of trout farms, MG in effluent water ranged from 5.65 ng/L to 384 μg/L, and fish tissue from the same sites contained 265–1663 μg/kg [5]. The 0.1–10 μg/L range examined here lies within the range reported for effluent water and thus corresponds to the elevated levels that follow shortly after illegal application, whereas the ng/L-level residues at the lower end of the reported range lie below the concentrations examined in this work.

The reliability of the quantification was corroborated by spike recovery experiments performed in triplicate at three concentration levels (1, 5 and 10 μg/L; Table 3). Recoveries of 89.6–100.9% with RSDs of 3.7–9.1% were obtained across the tested range. The absence of a detectable native MG signal in the blank samples, together with the near-quantitative recovery in spiked samples, demonstrates that matrix components in fishpond water do not significantly suppress or bias the SERS response of MG on the AuNRs-MIL-100(Fe) substrate. These results establish that trace MG in complex aquaculture water can be determined reliably by the present method. The advantage of the present substrate lies not in a lower detection limit but in its direct operation in untreated fishpond water, whereas several of the systems listed require extraction, pre-concentration or an imprinted recognition layer.

The selectivity of the method warrants explicit discussion, as MG belongs to the triphenylmethane family together with crystal violet (CV), brilliant green and leucomalachite green (LMG), all of which may co-occur in aquaculture environments. MG and CV differ by a single dimethylamino group and consequently exhibit closely matching SERS spectra, with corresponding marker bands near 800, 915, 1170 and 1615 cm^{-1} [13,48]. Chen et al. reported that MG, CV and their 1:1 mixture in fish could be resolved on standing AuNR substrates only after PCA/PLSR treatment of the spectra [13], which highlights that discrim-

ination between these congeners is not achievable from peak positions alone. This limitation is further relevant here because MIL-100(Fe) binds cationic triphenylmethane dyes strongly through electrostatic attraction and π–π stacking, with a reported CV uptake as high as 118.9 mg/g [49]; a coexisting dye may therefore compete with MG for the available binding sites. Accordingly, the 1617 cm^{-1} band is reliable for the quantification of MG under the conditions examined, but cannot by itself establish molecular identity when such congeners are present. Extending the platform to multi-analyte discrimination by chemometric or machine-learning approaches [13,50], or towards molecular imprinting, which has been used to suppress non-specific recognition for other targets [51], is a natural direction for future work.

Table 3. Recovery and RSD of malachite green spiked water samples on AuNRs-MIL-100(Fe).

Spiked (μg/L)	Recovery %	RSD %
1	96.7%	3.7%
5	89.6%	6.2%
10	100.9%	9.1%

4. Conclusions

In this study, AuNRs of three aspect ratios (2.4, 2.85 and 3.99) were synthesised by a seed-mediated route, and their growth mechanism and structure were characterised systematically. Silver nitrate acted as an auxiliary growth regulator whose dosage governs the aspect ratio, and the resulting aspect ratio sets the position of the longitudinal plasmon band. Among the three substrates, the AR 3.99 rods gave the strongest SERS enhancement, and their integration with MIL-100(Fe) produced a signal 56% stronger than that of the spherical AuNPs-MIL-100(Fe) counterpart at the same gold concentration; this substrate was therefore selected for all further work. The optimised substrate responded linearly to MG from 0.1 to 10 μg/L, with an intra-batch RSD of 19.2% and an inter-batch RSD of 12.9%. Applied directly to fishpond water without extraction or pre-concentration, it gave $R^2 = 0.966$ and spike recoveries of 89.6–100.9% with RSDs of 3.7–9.1%. The 0.1–10 μg/L range examined covers the elevated MG levels reported in a trout-farm survey of aquaculture effluent [5], although residues at the ng/L level lie below the concentrations examined in this work. The 1617 cm^{-1} band is reliable for quantifying MG under these conditions, although it cannot by itself establish molecular identity when structurally related triarylmethane dyes are present. The method thus combines acceptable reproducibility with direct analysis of untreated water, and the rational pairing of an anisotropic plasmonic nanostructure with a porous MOF offers a practical route to next-generation SERS substrates for multi-analyte and on-site environmental monitoring.

Author Contributions: Y.O.: Investigation, Formal analysis, and writing—original draft. J.C.: Conceptualization, data curation, Writing—review and editing. Y.S.: Software and data curation, Conceptualization, Resources. K.L.: Conceptualization, Resources, Supervision, Project administration, Writing—review and editing. All authors have read and agreed to the published version of the manuscript.

Funding: This study was funded by the National Natural Science Foundation of China (32272391) and the Natural Science project of Shanghai Zhongqiao Vocational and Technical University (2025ZQZR52).

Data Availability Statement: The original contributions presented in this study are included in the article. Further inquiries can be directed to the corresponding author.

Conflicts of Interest: The authors declare no conflicts of interest.

References

1. Srivastava, S.; Sinha, R.; Roy, D. Toxicological effects of malachite green. *Aquat. Toxicol.* **2004**, *66*, 319–329. [CrossRef] [PubMed]
2. Sudova, E.; Machova, J.; Svobodova, Z.; Vesely, T. Negative effects of malachite green and possibilities of its replacement in the treatment of fish eggs and fish: A review. *Vet. Med.* **2007**, *52*, 527–539. [CrossRef]
3. Fang, X.; Yang, S.; Chingin, K.; Zhu, L.; Zhang, X.; Zhou, Z.; Zhao, Z. Quantitative detection of trace malachite green in aquiculture water samples by extractive electrospray ionization mass spectrometry. *Int. J. Environ. Res. Public Health* **2016**, *13*, 814. [CrossRef] [PubMed]
4. *GB/T 19857-2005*; Determination of Malachite Green and Crystal Violet Residues in Aquatic Product. Standardization Administration of the People's Republic of China: Beijing, China, 2005.
5. Khodabakhshi, A.; Amin, M. Determination of malachite green in trout tissue and effluent water from fish farms. *Int. J. Environ. Health Eng.* **2012**, *1*, 10. [CrossRef]
6. Safarik, I.; Safarikova, M. Detection of low concentrations of malachite green and crystal violet in water. *Water Res.* **2002**, *36*, 196–200. [CrossRef] [PubMed]
7. Jin, Y.; Ma, P.; Liang, F.; Gao, D.; Wang, X. Determination of malachite green in environmental water using cloud point extraction coupled with surface-enhanced Raman scattering. *Anal. Methods* **2013**, *5*, 5609–5614. [CrossRef]
8. Kan, C.; Zhu, J.; Zhu, X. Silver nanostructures with well-controlled shapes: Synthesis, characterization and growth mechanisms. *J. Phys. D. Appl. Phys.* **2008**, *41*, 155304. [CrossRef]
9. Qin, M.; Wang, C.; Zhu, J.; Yong, L.; Wang, H.; Yang, L. Synthesis of differently sized gold nanoparticles for SERS applications in the detection of malachite green. *Spectroscopy* **2021**, *36*, 41–54.
10. Li, Z.H.; Bai, J.H.; Zhang, X.; Lv, J.M.; Fan, C.S.; Zhao, Y.M.; Wu, Z.L.; Xu, H.J. Facile synthesis of Au nanoparticle-coated Fe3O4 magnetic composite nanospheres and their application in SERS detection of malachite green. *Spectrochim. Acta Part A Mol. Biomol. Spectrosc.* **2020**, *241*, 118532. [CrossRef] [PubMed]
11. Liu, Y.; Li, J.; Liu, Q.; Weng, G.J.; Zhu, J.; Zhao, J.W. Sensitive detection of malachite green in aquaculture water by surface enhanced Raman scattering using silver coated urchin-like gold nanoparticles. *Colloids Surf. A Physicochem. Eng. Asp.* **2023**, *668*, 131485. [CrossRef]
12. Zhang, H.; Sun, D.; Wen, Y.; Wang, M.; Huang, J.; Lian, Z.; Li, J. Molecularly imprinted SERS plasmonic sensor for the detection of malachite green. *Biosensors* **2025**, *15*, 329. [CrossRef] [PubMed]
13. Chen, X.; Nguyen, T.H.D.; Gu, L.; Lin, M. Use of standing gold nanorods for detection of malachite green and crystal violet in fish by SERS. *J. Food Sci.* **2017**, *82*, 1640–1646. [CrossRef] [PubMed]
14. Zong, C.; Xu, M.; Xu, L.; Wei, T.; Ma, X.; Zheng, X.S.; Hu, R.; Ren, B. Surface-enhanced Raman spectroscopy for bioanalysis: Reliability and challenges. *Chem. Rev.* **2018**, *118*, 4946–4980. [CrossRef] [PubMed]
15. Luo, M.; Qin, L.; Tao, J.; Gao, X.; Zhang, T.; Kang, S.Z.; Li, X. Selective surface enhanced Raman detection and effective photocatalytic degradation of sulfonamides antibiotic based on a flexible three-dimensional chitosan/carbon nitride/silver substrate. *J. Hazard. Mater.* **2023**, *459*, 132131. [CrossRef] [PubMed]
16. Chen, X.; Wang, D.; Li, J.; Xu, T.; Lai, K.; Ding, Q.; Lin, H.; Sun, L.; Lin, M. A spectroscopic approach to detect and quantify phosmet residues in Oolong tea by surface-enhanced Raman scattering and silver nanoparticle substrate. *Food Chem.* **2020**, *312*, 126016. [CrossRef] [PubMed]
17. He, J.; Song, G.; Wang, X.; Zhou, L.; Li, J. Multifunctional magnetic Fe3O4/GO/Ag composite microspheres for SERS detection and catalytic degradation of methylene blue and ciprofloxacin. *J. Alloys Compd.* **2022**, *893*, 162226. [CrossRef]
18. Huang, C.; Li, A.; Chen, X.; Wang, T. Understanding the role of metal-organic frameworks in surface-enhanced Raman scattering application. *Small* **2020**, *16*, 2004802. [CrossRef] [PubMed]
19. Li, D.; Cao, X.; Zhang, Q.; Ren, X.; Jiang, L.; Li, D.; Deng, W.; Liu, H. Facile in situ synthesis of core–shell MOF@Ag nanoparticle composites on screen-printed electrodes for ultrasensitive SERS detection of polycyclic aromatic hydrocarbons. *J. Mater. Chem. A* **2019**, *7*, 14108–14117. [CrossRef]
20. Xu, H.; Zhu, J.; Wu, X.; Cheng, Y.; Wang, D.; Cai, D. Recognition and quantitative analysis for six phthalate esters (PAEs) through functionalized ZIF-67@Ag nanowires as surface-enhanced Raman scattering substrate. *Spectrochim. Acta Part A Mol. Biomol. Spectrosc.* **2023**, *284*, 121735. [CrossRef] [PubMed]
21. Chen, G.; Guan, M.; Yang, Z.; Mi, F.; Wang, Y.; Rao, X. High adsorption separation capacity magnetic MOF-based substrate Fe3O4@ZIF-67@Ag for sensitive and recyclable SERS detection of malachite green in aquaculture. *Microchem. J.* **2024**, *207*, 112098. [CrossRef]
22. Nandi, S.; Dalapati, R. Fluorometric sensing of arsenic in water: Recent developments in metal-organic framework-based sensors. *Processes* **2025**, *13*, 923. [CrossRef]
23. Ai, B.; Luo, M.; Khan, I. Effective malachite green degradation over the noble metal-doped and MOF-coupled CsSnBr3 nanocomposite catalyst. *Processes* **2023**, *11*, 1398. [CrossRef]

24. Ribeiro, I.S.; Aquino, W.C.P.; Alfredo, L.H.M.; de Jesus, J.R. Metal-organic frameworks as multifunctional platforms for chemical sensors: Advances in electrochemical and optical detection of emerging contaminants. *Processes* **2026**, *14*, 886. [CrossRef]
25. Yang, Y.; Matsubara, S.; Xiong, L.; Hayakawa, T.; Nogami, M. Solvothermal synthesis of multiple shapes of silver nanoparticles and their SERS properties. *J. Phys. Chem. C* **2007**, *111*, 9095–9104. [CrossRef]
26. Chen, H.; Shao, L.; Li, Q.; Wang, J. Gold nanorods and their plasmonic properties. *Chem. Soc. Rev.* **2013**, *42*, 2679–2724. [CrossRef] [PubMed]
27. Carbo-Argibay, E.; Rodriguez-Gonzalez, B.; Pastoriza-Santos, I.; Perez-Juste, J.; Liz-Marzan, L.M. Growth of pentatwinned gold nanorods into truncated decahedra. *Nanoscale* **2010**, *2*, 2377–2383. [CrossRef] [PubMed]
28. Wang, D.; Hore, M.; Ye, X.; Zheng, C.; Murray, C.B.; Composto, R.J. Gold nanorod length controls dispersion, local ordering, and optical absorption in polymer nanocomposite films. *Soft Matter* **2014**, *10*, 3404–3413. [CrossRef] [PubMed]
29. Guo, X.; Ye, W.; Zhu, R.; Wang, W.; Xie, F.; Sun, H.; Zhao, Q.; Ding, Y.; Yang, J. Gold nanorod-templated synthesis of polymetallic hollow nanostructures with enhanced electrocatalytic performance. *Nanoscale* **2014**, *6*, 11732–11737. [CrossRef] [PubMed]
30. Sancı, R.; Volkan, M. Surface-enhanced Raman scattering (SERS) studies on silver nanorod substrates. *Sens. Actuators B Chem.* **2009**, *139*, 150–155. [CrossRef]
31. Ju, J.; Byeon, E.; Han, Y.; Kim, S.M. Fabrication of a substrate for Ag-nanorod metal-enhanced fluorescence using the oblique angle deposition process. *Micro Nano Lett.* **2013**, *8*, 370. [CrossRef]
32. Han, H.Y.; Huang, Y.Q.; Miao, J.J.; Lai, K.Q. Rapid determination of malachite green in fish by surface-enhanced Raman spectroscopy combined with MIL-100(Fe). *Microchim. Acta* **2025**, *192*, 185. [CrossRef] [PubMed]
33. Shen, Y.; Liang, L.; Zhang, S.; Huang, D.; Zhang, J.; Xu, S.; Liang, C.; Xu, W. Organelle-targeting surface-enhanced Raman scattering (SERS) nanosensors for subcellular pH sensing. *Nanoscale* **2018**, *10*, 1622–1630. [CrossRef] [PubMed]
34. Walsh, M.; Barrow, S.; Tong, W.; Funston, A.M.; Etheridge, J. Symmetry breaking and silver in gold nanorod growth. *ACS Nano* **2015**, *9*, 715–724. [CrossRef] [PubMed]
35. Gao, J.; Bender, C.; Murphy, C. Dependence of the gold nanorod aspect ratio on the nature of the directing surfactant in aqueous solution. *Langmuir* **2003**, *19*, 9065–9070. [CrossRef]
36. Murphy, C.; San, T.; Gole, A.; Orendorff, C.J.; Gao, J.; Gou, L.; Hunyadi, S.E.; Li, T. Anisotropic metal nanoparticles: Synthesis, assembly, and optical applications. *J. Phys. Chem. B* **2005**, *109*, 13857–13870. [CrossRef] [PubMed]
37. Murphy, C.; Thompson, L.; Chernak, D.; Yang, J.A.; Sivapalan, S.T.; Boulos, S.P.; Huang, J.; Alkilany, A.M.; Sisco, P.N. Gold nanorod crystal growth: From seed-mediated synthesis to nanoscale sculpting. *Curr. Opin. Colloid Interface Sci.* **2011**, *16*, 128–134. [CrossRef]
38. Naujok, R.; Duevel, R.; Corn, R. Fluorescence and Fourier transform surface-enhanced Raman scattering measurements of methylene blue adsorbed onto a sulfur-modified gold electrode. *Langmuir* **1993**, *9*, 1771–1774. [CrossRef]
39. Yao, I.; Chang, C.; Ko, H.; Li, H.; Lu, T.C.; Chen, J.T. Rapid separation of gold nanorods in multilayer aqueous systems via centrifugation. *RSC Adv.* **2016**, *6*, 90786–90791. [CrossRef]
40. Tong, W.; Walsh, M.; Mulvaney, P.; Etheridge, J.; Funston, A.M. Control of symmetry breaking size and aspect ratio in gold nanorods: Underlying role of silver nitrate. *J. Phys. Chem. C* **2017**, *121*, 3549–3559. [CrossRef]
41. Chen, M.; Huang, Y.; Miao, J.; Fan, Y.; Lai, K. A highly sensitive surface-enhanced Raman scattering sensor with MIL-100(Fe)/Au composites for detection of malachite green in fish pond water. *Spectrochim. Acta Part A Mol. Biomol. Spectrosc.* **2023**, *292*, 122432. [CrossRef] [PubMed]
42. Gole, A.; Orendorff, C.J.; Murphy, C.J. Immobilization of gold nanorods onto acid-terminated self-assembled monolayers via electrostatic interactions. *Langmuir* **2004**, *20*, 7117–7122. [CrossRef] [PubMed]
43. He, J.; Zhang, H.; Zhu, J.; Zhang, X.; Liu, X.; Ramachandraiah, K.; Ke, F. Layer-by-layer synthesis of Au nanorods@metal-organic framework core-shell nanohybrids for magnetic resonance imaging guided photothermal therapy. *Mater. Today Commun.* **2022**, *33*, 104560. [CrossRef]
44. Le Ru, E.C.; Etchegoin, P.G. Rigorous justification of the |E|4 enhancement factor in surface enhanced Raman spectroscopy. *Chem. Phys. Lett.* **2006**, *423*, 63–66. [CrossRef]
45. Orendorff, C.J.; Gearheart, L.; Jana, N.R.; Murphy, C.J. Aspect ratio dependence on surface enhanced Raman scattering using silver and gold nanorod substrates. *Phys. Chem. Chem. Phys.* **2006**, *8*, 165–170. [CrossRef] [PubMed]
46. Park, W.; Huh, Y.; Hong, W. Aspect-ratio-controlled synthesis of high-aspect-ratio gold nanorods in high-yield. *Curr. Appl. Phys.* **2009**, *9*, e140–e143. [CrossRef]
47. Fateixa, S.; Correia, M.; Trindade, T. Resizing of colloidal gold nanorods and morphological probing by SERS. *J. Phys. Chem. C* **2013**, *117*, 20343–20350. [CrossRef]
48. Song, J.; Huang, Y.; Fan, Y.; Zhao, Z.; Yu, W.; Rasco, B.A.; Lai, K. Detection of prohibited fish drugs using silver nanowires as substrate for surface-enhanced Raman scattering. *Nanomaterials* **2016**, *6*, 175. [CrossRef] [PubMed]

49. Zhang, J.; Li, R.; Wen, Y.; Li, Y.; Yang, Y.; Wang, H.; Yang, Y.; Tai, Z. One-pot synthesis of nanosized magnetic MIL-100(Fe) with abundant defects and its application in the adsorption of triphenylmethane dyes. *Inorg. Chem. Commun.* **2026**, *184*, 115934. [CrossRef]
50. Guhlke, M.; Heiner, Z.; Kneipp, J. Surface-enhanced hyper-Raman and Raman hyperspectral mapping. *Phys. Chem. Chem. Phys.* **2016**, *18*, 14228–14233. [CrossRef] [PubMed]
51. Chen, X.; Ostovan, A.; Arabi, M.; Wang, Y.; Chen, L.; Li, J. Molecular imprinting-based SERS detection strategy for the large-size protein quantitation and curbing non-specific recognition. *Anal. Chem.* **2024**, *96*, 6417–6425. [CrossRef] [PubMed]

Disclaimer/Publisher's Note: The statements, opinions and data contained in all publications are solely those of the individual author(s) and contributor(s) and not of MDPI and/or the editor(s). MDPI and/or the editor(s) disclaim responsibility for any injury to people or property resulting from any ideas, methods, instructions or products referred to in the content.